

Comparative study between PMSM models used for NVH system-level simulation

Jose Enrique Ruiz Sarrió
Engineering Services RTD
Siemens Industry Software NV
Leuven, Belgium

Department of Electrical
Machines and Drives
Technical University of Cluj-Napoca
Cluj-Napoca, Romania
jose.ruiz_sarrio@siemens.com

Claudia Martis
Department of Electrical
Machines and Drives
Technical University of Cluj-Napoca
Cluj-Napoca, Romania

Sebastian Ciceo
Engineering Services RTD
Siemens Industry Software NV
Leuven, Belgium

Department of Electrical
Machines and Drives
Technical University of Cluj-Napoca
Cluj-Napoca, Romania

BEAMS Department,
Electrical Energy Group
Université Libre de Bruxelles
Brussels, Belgium

Fabien Chauvicourt
Engineering Services RTD
Siemens Industry Software NV
Leuven, Belgium

Abstract— Modeling of automotive Permanent Magnet Synchronous Machines (PMSM) electric drives for Noise, Vibration and Harshness (NVH) assessment involves modeling different components such as electrical machine, power electronics and controller. The usage of transistors for machine control affects the NVH performance, especially within the switching frequency range. Traditionally the method to include power electronics models is to use co-simulation to couple a circuit simulator with an electromagnetic Finite Element (FE) model. However, this approach is computationally expensive. To overcome this limitation, the electromagnetic behavior of the machine can be approximated by using reduced order models. This work compares the co-simulation approach with the system-level model in terms of high frequency NHV behavior. The comparison provides results in terms of time and accuracy.

Keywords— PMSMs, NVH, system-level simulation, reduced order modeling, co-simulation

I. INTRODUCTION

Electrical machines in automotive industry are more and more popular in the latest years. Not only the powertrain now includes this technology, but also many auxiliary systems such as steering systems, air conditioning compressors or braking systems [1]. In this context, one of the most extensively used type of electrical machines is the Permanent Magnet Synchronous Machines (PMSMs) due to its high power density compared to other machine typologies.

One important performance criteria is the Noise, Vibrations and Harshness (NVH) behavior. To predict it, and especially within an early-design stage, system-level (SL) modeling strategies are usually implemented. This, essentially results from the multi-physical characteristic of noise and vibrations (control, structural dynamics, electromagnetics). Previous work on the SL simulation approaches can be found on [2], [3].

However, SL studies can become computationally expensive depending on the modelling strategy. Focusing on the PMSM electromagnetic model, non-linear phenomena such as slotting effects and saturation of the iron core, affect the machine behavior. This typically leads to the usage of Finite Element (FE) methods, which take into account non-linearities. This approach is considered to be computationally expensive. Reduced Order Models (ROMs) have been developed to simplify NVH simulation. The ROMs map several machine characteristics reducing the computational time. This is achieved by an input/output block, based on Look-up Tables (LUTs). A series of current-fed magnetostatic FE analysis are performed and machine parameters (i.e. flux-linkages plus electromagnetic torque [4], co-energy [5], etc.) are stored on the LUTs.

Realistic conditions are set for on-line simulations by including power electronics models, which impose voltage on the machine terminals. Pulse Width Modulation (PWM) techniques are typically employed in order to control the machine and to consider switching frequency effects [6]. The current flowing in the windings is obtained from the governing equations of the machine and the B-field on the air gap, which is obtained in parallel. The radial component of this B-field is responsible for the generation of the radial force spectra, which is the main excitation source for noise and vibration in electrical machines.

This work compares two PMSM models regarding their high-frequency electromagnetic behavior for NVH simulations. In order to carry out the comparison, two simulation schemes are defined as depicted in Figure 1. The first model is a SL, reduced order model with flux-linkages data store in 3D LUTs. The second one is a 2D FE model.

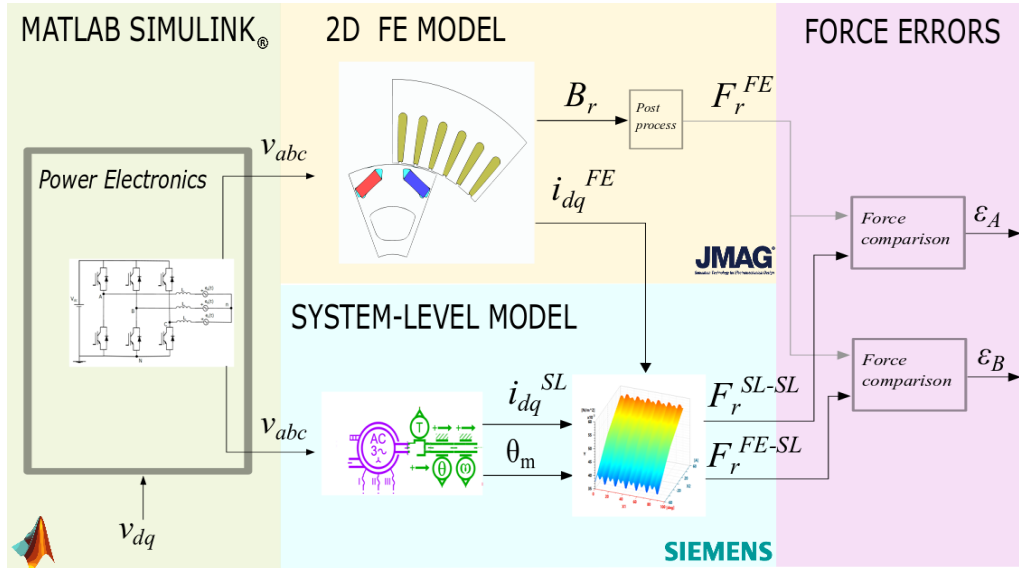


Fig. 1. Block diagram of method used for model comparison

The power electronics model for PWM feeding is implemented for both approaches. Section II describes the models under comparison and, in Section III, the simulation procedure is explained and results are presented and discussed.

II. SIMULATION MODELS

A. System-level Model

In this approach, the machine model is a reduced order model based on LUTs. Flux-linkage values are stored in LUTs by running a series of magnetostatic FE simulations. The coils flux-linkage is obtained for different values of the rotor position θ_m , and the currents in the dq reference frame, i_d and i_q . Thus, it is possible to obtain two LUTs of the dq -referenced flux-linkages ψ_d, ψ_q , as functions of the currents and the electrical angle θ_e : $\psi_d = f(i_d, i_q, \theta_e)$ and $\psi_q = f(i_d, i_q, \theta_e)$.

Machine currents are then obtained during dynamic simulation by using [2]:

$$\begin{bmatrix} \frac{di_d}{dt} \\ \frac{di_q}{dt} \end{bmatrix} = \begin{bmatrix} \frac{d\psi_d}{di_q} & \frac{d\psi_q}{di_d} \\ \frac{d\psi_d}{di_d} & \frac{d\psi_q}{di_q} \end{bmatrix}^{-1} \cdot \left(\begin{bmatrix} v_d \\ v_q \end{bmatrix} - R \begin{bmatrix} i_d \\ i_q \end{bmatrix} - \begin{bmatrix} \psi_d + \frac{d\psi_q}{d\theta_e} \\ -\psi_q + \frac{d\psi_d}{d\theta_e} \end{bmatrix} \omega_e \right) \quad (1)$$

where v_d and v_q are the imposed voltage on d-axis and q-axis respectively, R is the winding resistance and θ_e and ω_e represent the electrical angle and speed. By solving Eq. (1) during the on-line simulation, the solution for the machine currents is obtained for every time step.

The radial component of the B-field in the air gap depends on the rotor position for each time step and on its spatial distribution along the air gap geometry. The radial force spectra is obtained from the B-field by using the Maxwell Stress Tensor [7]. Fourier series decomposition is applied to the radial force to isolate the spatial and the rotor position dependent components. This procedure allows to simplify the analysis within SL model simulation and it is performed for each operating point following [3], [8]:

$$F(t, \alpha) = \sum_{\nu=-M}^M F_m(t, \alpha) = F_0(t) + \sum_{\nu=1}^M F_{\cos, \nu}(t) \cos(\nu\alpha) + \sum_{\nu=-1}^{-M} F_{\sin, -\nu}(t) \sin(\nu\alpha) \quad (2)$$

where M is the number of considered space orders, ν is the ν^{th} space order, α is the angle along the air gap. The main spatial orders are given by the greatest common divider between the number of slots and twice the number of pole pairs [7].

The force shapes amplitude factors can be stored in 3D LUTs depending on i_d, i_q and the mechanical angle θ_m : $F_0 = f(i_d, i_q, \theta_m)$, $F_{\cos, \nu} = f(i_d, i_q, \theta_m)$, $F_{\sin, \nu} = f(i_d, i_q, \theta_m)$.

A cubic interpolation method is used for acquisition of both flux-linkages and force data.

B. 2D FE transient model

For the machine FE transient analysis, voltage is imposed on the windings circuit and then, it is translated into current density on the machine conductors which contribute to the generation of the total B-field. The current density on the conductors together with the field originated by the permanent magnets in the rotor, define the radial flux density in the air gap of the machine. The radial component of this field is extracted for each rotor position along the geometry of the air gap. Radial forces are calculated according to the Maxwell Stress Tensor [7] and by post-processing the data, the Fourier decomposition in Eq. (2) is achieved. In this way, the amplitude factors for each rotor position ($F_0, F_{\cos, \nu}, F_{\sin, \nu}$) are obtained for each operating point under consideration.

III. MODEL COMPARISON AND ANALYSIS

The machine considered for model comparison is a three-phase, V-shaped, Y-connected with floating neutral, 48-slot-8-pole, Interior Permanent Magnet Synchronous Machine (IPMSM). Table I shows the main machine characteristics and Figure 2 depicts its cross-section. A three-phase, two-level, voltage source inverter is used for machine feeding.

TABLE I. IPMSM CHARACTERISTICS

Parameter	Unit	Value
Peak power rating	kW	60
Peak torque	Nm	207
Base rotational speed	rpm	3000
Stator outer diameter	mm	64
Stator stack length	mm	50.8
Air gap length	mm	0.73

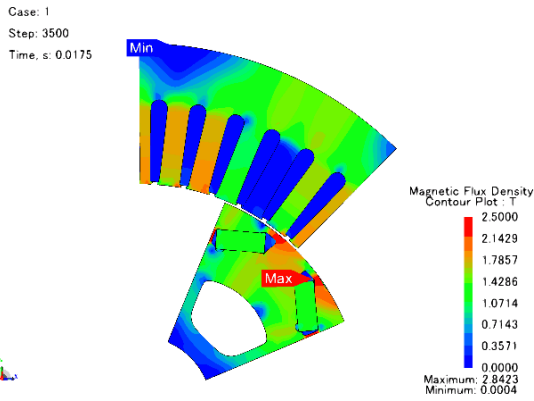


Fig. 2. Cross-section of the machine with B-field contour plot ($t=0.0175$)

The motor is fed in open-loop since it is sufficient to obtain the electromagnetic behavior of the machine. Moreover, the two different models have slightly different dynamic behavior and thus, an extra error is added under closed-loop control.

Imposed speed is 3000 rpm and the switching frequency f_{sw} is equal to 10 kHz. A set of 5 operating points imposing the same speed is defined by using null and negative values of i_d . Table II defines the considered operating points for stable conditions in open-loop operation.

The first result is found in terms of computational time difference. The SL model requires the acquisition of data for building the 3D LUTs. This process is performed off-line, thus, it is only required once for each machine model. For the present work 7 break points are selected for both i_d and i_q , which results on 49 FE simulations with an actual simulation time of 20 minutes each. The total simulation time for obtaining the 3D LUTs data is around 16 hours and 33 minutes.

For on-line simulation of one electrical period (0.005 seconds for the imposed speed), the simulation time for the 2D FE model co-simulation is 8 minutes, while for the SL approach is 9.7 seconds. These results confirm that the SL model is approximately 50 times faster than the co-simulation approach. Nevertheless, when analysis of a small amount of operating points is required, the SL approach does not incur in a significant time save.

TABLE II. OPERATING POINTS

Operating point	$i_d i_q$	v_{dq}
OP1	zero, high	-350, 210 V
OP2	zero, low	-160, 207.5 V
OP3	high, high	-350, 97 V
OP4	low, low	-150, 185 V
OP5	high, low	-100, 40 V

A. PWM modulated input voltage

The voltage signal is imposed by the three-phase inverter with PWM modulation. The leg-voltages v_{AN} , v_{BN} , and v_{CN} (between one phase and the ground) are applied on the machine phase terminals. Due to the floating neutral of the machine, the voltage drops on the windings will not be equal to the leg-voltages and their per-phase expression will be given by [9]:

$$v_{An}(t) = \frac{2}{3} v_{AN} - \frac{1}{3} (v_{BN}(t) + v_{CN}(t)) \quad (3)$$

where v_{AN} , v_{BN} and v_{CN} are the three-phase voltage drops in the machine windings. Figure 3 shows the leg and phase-voltages together with their high-frequency harmonic spectra.

The most significant harmonic orders of the phase-voltage signal are located on $6k \pm 1$ times the fundamental frequency f_1 (baseband harmonics) and around multiples of the main switching frequency f_{sw} (sideband harmonics) [6], [10].

B. Machine currents comparison

Errors between current signals are expected and they depend on the accuracy of the interpolation method and the amount of break-points of the LUTs. Figure 4 shows the differences in i_{dq} between both SL and 2D FE models in time domain.

The most significant harmonics of the phase-current are coincident with the phase-voltage ones. The high-frequency spectra is composed by the sideband components around the switching frequency f_{sw} . Figure 5 shows the amplitude comparison for the high-frequency harmonics range. Table III shows results for the absolute value differences and the relative error for each component. For relative error computation, the values obtained on the 2D FE model co-simulation are considered as the reference.

The fundamental component f_1 is the same for every operating point since they share the same imposed speed. Thus, the harmonic components in the switching frequency range for every operating point also share the same positions. Due to this fact, the comparison can be extended in order to compare the harmonic amplitude differences along the operating regions of the machine.

TABLE III. PHASE-CURRENT HIGH-FREQUENCY HARMONICS AMPLITUDE COMPARISON

Harmonic orders	$ I_a^{FE} - I_a^{SL} $	Rel. error (%)
$f_{sw} - 4f_1$	0.013 A	1.224
$f_{sw} - 2f_1$	0.015 A	0.787
$f_{sw} + 2f_1$	0.015 A	1.046
$f_{sw} + 4f_1$	0.019 A	2.054
$2f_{sw} - 5f_1$	0.006 A	2.383
$2f_{sw} - f_1$	0.003 A	0.356
$2f_{sw} + f_1$	0.004 A	0.536
$2f_{sw} + 5f_1$	0.001 A	0.205

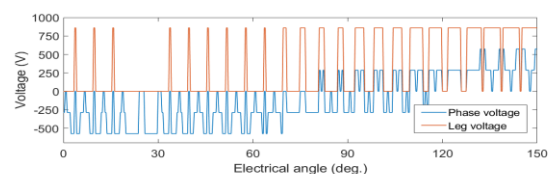


Fig. 3. Voltage signals and their high-frequency harmonic spectra (Point 1)

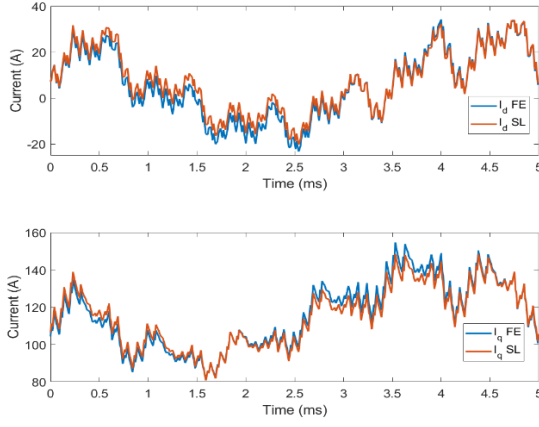
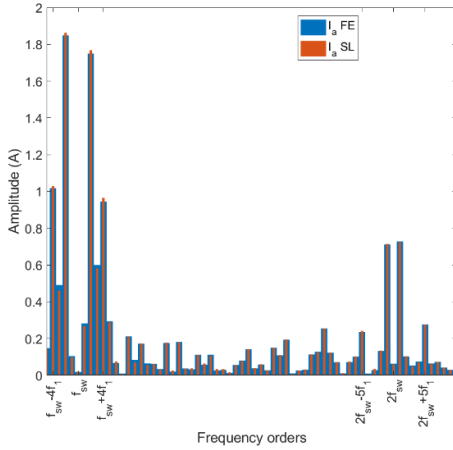
Fig. 4. i_{dq} time domain comparison (Point 1)

Fig. 5. Phase-current high-frequency harmonic spectra (Point 1)

Figure 6 shows a colormap depicting the absolute and relative errors on the sideband harmonics for each operating point. The last two rows of the colormaps represent the average value and the standard deviation.

Two trends are observed on the absolute error. The first one refers to the harmonic orders; the higher the harmonic order, the lower is the absolute error and the standard deviation. The second trend is observed on the amplitude of i_q (and thus, the amplitude of the phase-current); the higher i_q , the higher is the absolute error on the phase current. The maximum absolute error is 0.019 A for Point 1, where peak value of the current is 125 A (0.015 % relative error compared with the peak value).

Regarding the relative error, an outlier is found in the harmonic order $2f_{sw} + 5f_1$ of point 2, where the relative error is 45.89 %. In any case, the average values of the relative error do not overcome 15 %.

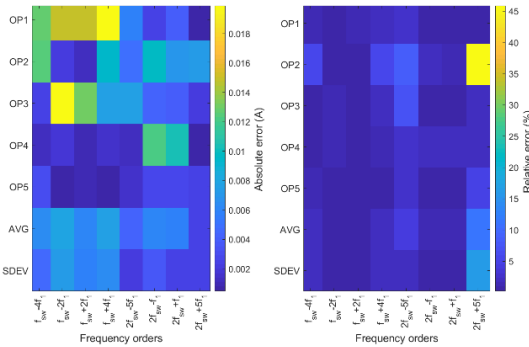


Fig. 6. Phase-current errors for different operating points

C. Radial forces comparison

The most significant force orders are identified by decomposing the force along the air gap for a single rotor position. Figure 7 shows the radial force signal and the superposition of the main force when truncation is applied at the 48th order. By decomposing the rotor position dependent terms on their Fourier series with respect to time, the harmonics for each amplitude factor are identified. Figure 8 shows the lower order force amplitude factors and their high frequency harmonic content. Truncation is applied on the 16th order since the higher order forces are negligible. For some operating points, the 0 order shape has an amplitude peak on $2f_{sw}$ which is not present for the conditions depicted on Figure 8.

Two types of error are defined for radial force comparison. Block diagram in Figure 1 shows the process for error computation. Error A (ϵ_A) avoids currents i_{dq} discrepancies and isolates the error on the forces data acquisition. Error B (ϵ_B) takes into account the deviation on the i_{dq} currents. Relative and absolute errors for both cases are given by:

$$\epsilon_A = |F_r^{FE} - F_r^{SL-SL}|; \bar{\epsilon}_A = \frac{|F_r^{FE} - F_r^{SL-SL}|}{F_r^{FE}} \quad (4)$$

$$\epsilon_B = |F_r^{FE} - F_r^{FE-SL}|; \bar{\epsilon}_B = \frac{|F_r^{FE} - F_r^{FE-SL}|}{F_r^{FE}} \quad (5)$$

where ϵ_A and ϵ_B represent the absolute error and $\bar{\epsilon}_A$ and $\bar{\epsilon}_B$ represent the relative. The radial force super indexes indicate the origin of the input current in the force LUTs. The term SL-SL indicates that the currents used for force calculation are obtained from the SL model. When FE-SL is used, it indicates that the current input in the LUTs is the output of the 2D FE model.

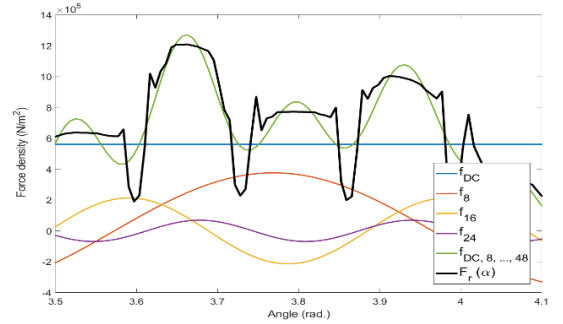


Fig. 7. Radial force spatial decomposition

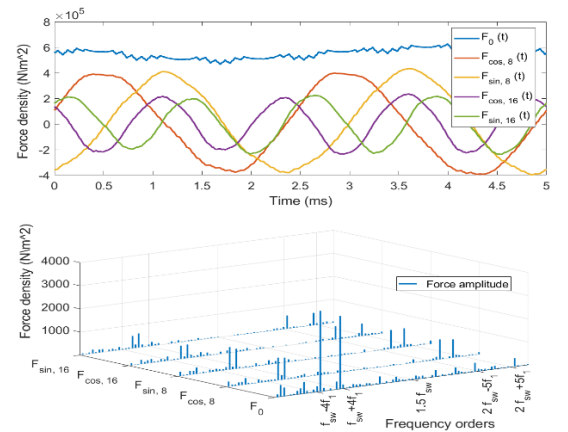


Fig. 8. Radial force amplitude factors and their high-frequency harmonic spectra

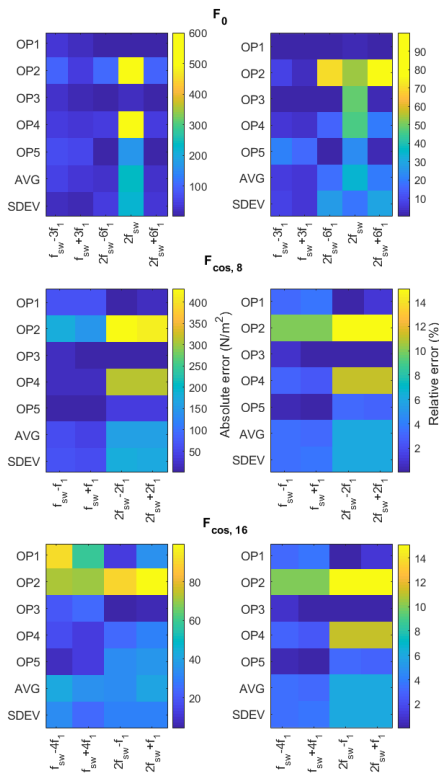


Fig. 9. Radial force amplitude factor errors for different operating points - Error A

Only one amplitude factor per order is considered for the comparison. The sinusoidal and co-sinusoidal waves of the same order provide the same information in terms of harmonic amplitudes. Thus, only the co-sinusoidal factors up to the 16th order are considered for comparison. Figure 9 and Figure 10 provide the absolute and relative errors for error A and error B respectively.

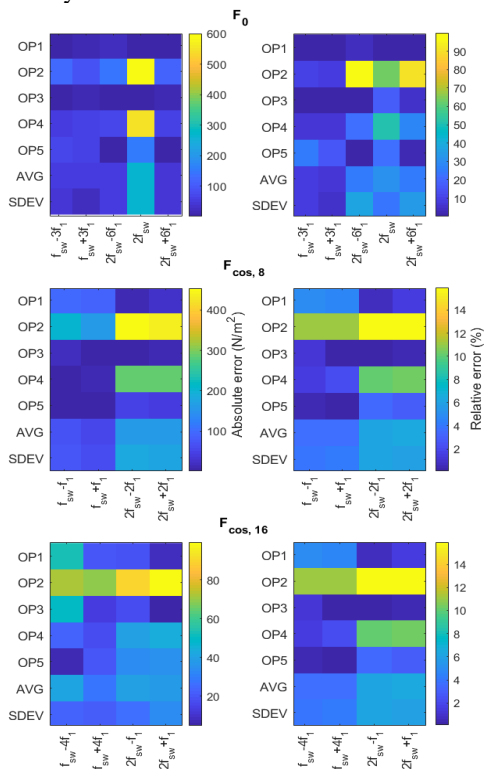


Fig. 10. Radial force amplitude factor errors for different operating points - Error B

The results show that the operating point 2 is the most discrepant. It coincides with the point having the less current amplitude. The harmonic at $2f_{sw}$ in the 0 order shape has the greatest difference in both absolute and relative error average values. The relative values reach up to 90% for the operating point 2, which confirms that outliers are present in the comparison. The differences of error A and error B are not significant since they follow the same trends. Error B is slightly minor in most of the cases.

IV. CONCLUSIONS

This paper compares two PMSM models when PWM modulated voltage is imposed. Discrepancies on current and radial force harmonic amplitudes are presented and discussed for five operating points of the machine. The analysis allows to identify the most discrepant harmonic components, and to evaluate the impact of the deviations on the high-frequency harmonic spectra. Further work on the topic would be focused on the expansion of the analysis using different type of data stored on LUTs (i.e. coenergy), and different interpolation methods. The sample of points considered can also be expanded to obtain more reliable statistical parameters. The analysis can be performed on different types of machine when their 2D FE model is available.

ACKNOWLEDGMENT

This paper is part of the European Industrial Doctorate on Next Generation for sustainable automotive Electrical Actuation (INTERACT) project which has received funding from the European Union Horizon 2020 research and innovation programme under grant agreement No 766180. Jose Enrique Ruiz Sarrió is an early stage researcher on this project. The authors would also like to acknowledge JSOL Corporation for granting access to JMAG software packages.

REFERENCES

- [1] B. Lenesque, "Automotive electrification: The nonhybrid story," *IEEE Trans. on Transportation Electrification*, vol. 1, no. 1, pp. 40-53, 2015.
- [2] S. Ciceo, F. Chauvicourt, J. Gyselinck, and C. Martis, "A comparative study of system-level PMSM models with either current or flux-linkage state variables used for vibro-acoustic computation," in *2019 IEEE International Electric Machines & Drives Conference (IEMDC)*, pp. 1881-1888, IEEE, 2019.
- [3] F. Chauvicourt, S. Ciceo, and H. Van der Auweraer, "On the use of vibration synthesis to ease electric machine powertrain design," in *2019 IEEE International Electric Machines & Drives Conference (IEMDC)*, pp. 1118-1125, IEEE, 2019.
- [4] G. Luo, R. Zhang, Z. Chen, W. Tu, S. Zhang, and R. Kennel, "A novel nonlinear modeling method for permanent-magnet synchronous motors," *IEEE Transactions on Industrial Electronics*, vol. 63, no. 10, pp. 6490-6498, 2016.
- [5] R. D. Schultz and L. Zhao, "Coenergy based transient model of interior permanent synchronous machines," in *2015 IEEE Industry Applications Annual Meeting*, pp. 1-7, IEEE, 2015.
- [6] T. Hara, T. Ajima, Y. Tanabe, M. Watanabe, K. Hoshino, and K. Oyama, "Analysis of vibration and noise in permanent magnet synchronous motors with distributed winding for the pwm method," *IEEE Transactions on Industry Applications*, vol. 54, no. 6, pp. 6042-6049, 2018.
- [7] J. F. Gieras, C. Wang, and J. C. Lai, *Noise of polyphase electric motors*. CRC press, 2018.
- [8] M. Bösing and R. W. de Doncker, "Acoustic modeling of electrical drives: noise and vibration synthesis based on force response superposition," tech. rep., Lehrstuhl und Institut für Stromrichtertechnik und Elektrische Antriebe, 2014.
- [9] N. Mohan and T. M. Undeland, *Power electronics: converters, applications, and design*. John Wiley & sons, 2007.
- [10] D. G. Holmes and T. A. Lipo, *Pulse width modulation for power converters: principles and practice*, vol. 18. John Wiley & sons, 2003.